optics

MDPI

Article

Comparison of Novel Raman Techniques for Fiber Forensics

Benjamin R. Anderson *, Natalie Gese and Hergen Eilers

Applied Sciences Laboratory, Institute for Shock Physics, Washington State University, Spokane, WA 99210-1495, USA; natalie.gese@wsu.edu (N.G.); eilers@wsu.edu (H.E.)
* Correspondence: branderson@wsu.edu

Abstract: We have proposed three novel Raman techniques to expand capabilities for non-destructive dyed-fiber forensics: THz Raman spectroscopy (TRS), integrating-cavity-enhanced Raman spectroscopy (ICERS), and deep-UV Raman spectroscopy (DUVRS). In this study, we report on our attempts to apply these techniques to a variety of dyed-nylon fibers and report on the results of each technique, with a particular focus on the dyes Acid Red 337 and Acid Yellow 49. We find that none of the dyes tested had discernible THz peaks but that they do impact the peak positions of the host fabric's THz spectrum. For ICERS, we find that light absorption overwhelms any possible cavity enhancement, making the technique unusable for most dyed fabrics when using UV/VIS excitation. However, NIR excitation may still prove beneficial, but a new cavity material (with a higher NIR reflectance) is needed. Finally, we tested DUVRS but found that, for all the dyed fibers tested, the DUV excitation resulted in rapid photodegradation, making the technique unusable for non-destructive forensics.

Keywords: Raman spectroscopy; forensics; Terahertz spectroscopy; integrating cavity; DUV Raman spectroscopy

check for updates

Citation: Anderson, B.R.; Gese, N.; Eilers, H. Comparison of Novel Raman Techniques for Fiber Forensics. *Optics* **2023**, *4*, 447–458. https://doi.org/10.3390/opt4030032

Academic Editor: Francesco Prudenzano

Received: 27 June 2023
Revised: 14 July 2023
Accepted: 25 July 2023
Published: 28 July 2023

1. Introduction

Collecting and analyzing trace evidence (e.g., fibers, hair, soil, wood, gunshot residue) is a standard practice during forensic investigations as it can be used to link a suspect to a victim, or link a suspect/victim to a location [1]. However, many of these investigative techniques are not well-developed and rely on non-rigorous techniques that do not have scientific support [2].

One such forensic field in need of further scientific development is trace fiber analysis. Currently, fiber analysis primarily focuses on the color of the fibers as the most important property [1,3]. Typically, this analysis begins with non-destructive approaches (e.g., light microscopy, Raman spectroscopy, and UV/VIS microspectrophotometry), and, if necessary, destructive approaches (e.g., thin-layer chromatography and gas chromatography mass spectrometry) are used [4–7]. The goal of these analyses is to determine the underlying dye blend that gives rise to a specific hue, which can then be compared to reference measurements to determine the fabric's origin and/or match to a sample belonging to a suspect or victim as needed. While this procedure is simple in theory, in practice, it faces a significant challenge in the fact that there are thousands of different dyes and dye mixtures that are used in preparing colored fabrics. This large set of possible dyes/mixtures makes it difficult to uniquely identify which dyes are actually present in any given sample, especially for non-destructive techniques.

Out of all the non-destructive techniques, the most promising approach is Raman spectroscopy [5,6,8–16] as Raman scattering signatures of dyes typically contain much narrower and unique peaks, whereas microscopy and UV/VIS spectrophotometry can struggle to differentiate between dyes as they rely on broad electronic transition. However, Raman spectroscopy also faces several major challenges: (1) Raman scattering efficiencies are tiny (on the order of 10^{-7}) [17], (2) most wavelengths for Raman spectroscopy also excite

fluorescence from the dyes, which is many orders of magnitude brighter than the Raman signal, (3) if too much laser intensity is used, the dyes photodegrade, resulting in new Raman spectra, and (4) mixtures of dyes can produce complicated spectra that are difficult to deconvolute due to the small signal from Raman scattering. To address these challenges, we have proposed applying three different novel Raman spectroscopy techniques to forensic fibers: Terahertz (THz) Raman spectroscopy (TRS), integrating-cavity-enhanced Raman spectroscopy (ICERS), and deep-UV Raman spectroscopy (DUVRS).

Terahertz (THz) Raman spectroscopy is a method to probe low-energy phonon modes of materials, typically with energies < 200 cm^{-1} [18]. A TRS setup is nearly identical to a standard Raman spectrometer, except, instead of using typical holographic notch filters (which have widths on the order of hundreds of cm^{-1}), they use specialized Bragg grating notch filters that can have notch widths on the order of 10 cm^{-1}. These narrow notch widths enable the capability to simultaneously probe structural information of materials (peaks below < 200 cm^{-1}) and chemical information (peaks > 200 cm^{-1}) [18]. In theory, the combination of these two pieces of information could help differentiate component dyes in mixtures.

The second proposed novel Raman technique is ICERS. ICERS was first demonstrated by Cone et al. [19] and involves using a highly reflecting integrating cavity to obtain cavity-enhanced Raman scattering due to multiple scattering of light inside the integrating cavity [19–23]. This technique is similar to traditional cavity-enhanced Raman spectroscopy [24], except, instead of using two highly reflecting mirrors—which are carefully aligned—ICERS uses a highly reflecting cavity, which drastically simplifies the setup and also reduces the cost. In theory, cavity enhancement could help significantly boost the Raman intensity while also lowering the peak intensity on the sample due to diffuse illumination. This combination would help produce greater signals with a lower risk of photodegradation.

Finally, DUV Raman spectroscopy is identical to traditional Raman, but, instead of using a visible or NIR laser for excitation, the technique uses a DUV laser at 266 nm, which requires special optics, gratings, and detectors. DUV excitation is desirable for Raman spectroscopy as its spectral range typically avoids a material's fluorescence emission and it is more intense due to the Raman intensity depending on λ^{-4} [25]. These features of DUV Raman spectroscopy have previously been used to interrogate a wide variety of other materials, including bacteria [26,27], chemical warfare agents [28], biochemical warfare agents [29], coal liquid [30], proteins [31,32], explosives [33], food/beverages [34], and other chemicals [35,36].

In this report, we compare the application of all three techniques to characterization of dyed-nylon fibers, with a special focus on Acid Red 337 and Acidy Yellow 49. These dyes were chosen as the main test dyes as they were found to have the best Raman characteristics of all the dyes tested. We find that, despite their promise, all three techniques face significant challenges, which limit their usefulness to non-destructive fiber forensics for dyed-nylon fibers.

2. Method

2.1. Samples

The dyed fabric samples tested in this study consisted of disperse dyes, reactive dyes, or acid dyes dispersed into either nylon, polyester, or cotton. Table 1 lists the different dyes with their respective hosts. The Permasil, Permabril, and Permalon dye samples were provided by Standard Colors, while the other samples were provided by Nelson Vinueza at North Carolina State University. Note that, while all these dyed fabrics were tested, we found that only the Acid Yellow 49 (AY49) and Acid Red 337 (AR337) dyed nylons provided us good data, with the rest of the samples displaying little to no Raman signal. Therefore, our discussion below will focus on these two dyed nylons and pristine nylon.

Table 1. List of dyed fabric swatches tested. Note: A. = acid, D. = disperse, R. = reactive.

Nylon Dyes	Polyester Dyes	Cotton Dyes
A. Black	Black Permasil	Black Permabril
A. Blue 62	Blue Permasil	Orange Permabril
A. Blue 260	Red Permasil	Red Permabril
A. Orance 67	Yellow Permasil	
A.Red 337 *	D. Red 153	
A. Yellow 49 *	D. Red 60	
Black Permalon	R. Blue 4	
Blue Permalon	R. Red 2	
Red Permalon	R. Red 123	
Yellow Permalon	R. Yellow 86	

* These dyes will be the samples for the rest of the paper.

2.2. THz Raman Spectroscopy

THz Raman spectroscopy (TRS) was performed using a setup consisting of a Coherent Verdi V5 Nd:YVO_4 laser (532 nm, 5 W, <5 MHz linewidth, RMS noise, 2%, 2 mm), a spatial filter, reflective Bragg grating ($\lambda_0 = 532$ nm, $\Delta\nu < 7$ cm^{-1}, 90% efficiency), beam steering optics, a Mitutoyo long working distance objective (20×, 0.40 NA, 20 mm WD), three Bragg notch filters ($\lambda_0 = 532$ nm, $\Delta\nu < 10$ cm^{-1}, OD3), a Princeton Instruments SP2500 monochromator (1800 g/mm, 500 nm blaze, 30 µm slit), and a Princeton Instruments Spec 10 CCD. See Figure 1 for a schematic of the TRS setup.

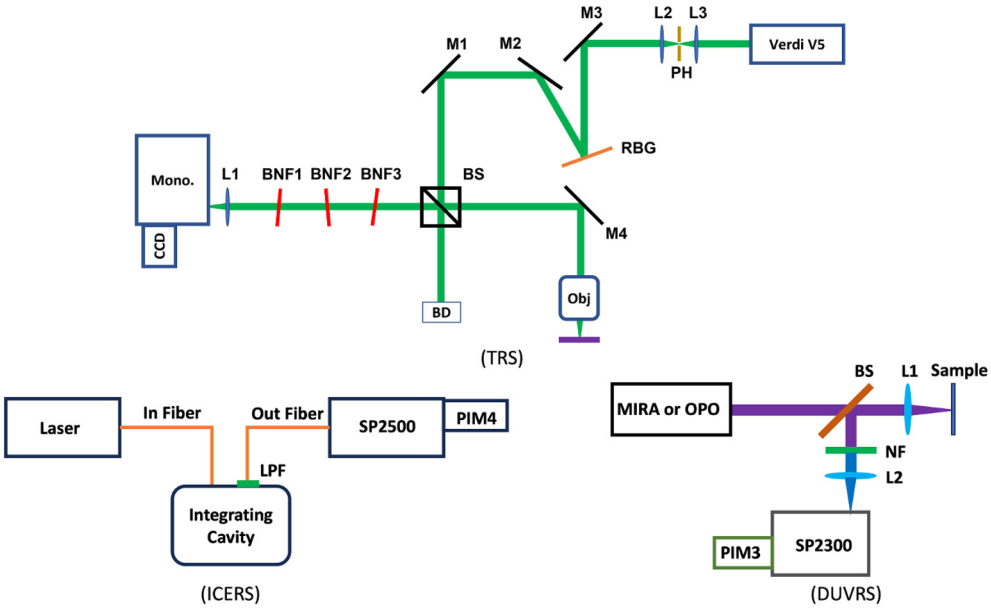

Figure 1. Experimental setups used for THz Raman spectroscopy (TRS), integrating-cavity-enhanced Raman spectroscopy (ICERS), and deep-UV Raman spectroscopy (DUVRS). BNF: Bragg notch filter, RBG: reflective Bragg grating, L: lens, M: mirrors, PH: pinhole, LPF: longpass filter, BS: beamsplitter.

2.3. ICERs

For integrating cavity preparation, we used Aerosil OX 50 (Evonik), which has very high reflectivity from 300 nm to 620 nm. See Figure 2 for example reflectance data. Poly(vinyl butyral-co-vinyl alcohol-co-vinyl acetate) (PVBVA) powder, average Mw 90,000–120,000, was used as a binder, 5% w/w with respect to Aerosil to aid with pressing and sintering. The PVBVA binder was combined with acetone (ACS grade) and the Aerosil to make a slurry. The PVBVA was first dissolved into acetone. Aerosil (20% w/w) was then added to the PVBA–acetone to make a slurry. The slurry was mixed for several hours to allow for PVBVA coating onto the Aerosil and then poured into shallow Pyrex

pans. The slurry was dried, crushed, coarse-sieved, and the resulting powder was pressed and heated to make cavity green bodies. For green body preparation, the powder was loaded into a 4-inch ID × 2-inch high cylinder made of polished fused quartz (Technical Glass Products). Approximately 135–250 g of the powder was packed and pressed between two quartz discs at approximately 318 psi (12.56-square-inch area) for 10 min. For the top and bottom segments of the cavity, 135 g of green powder was pressed. For the sections prepared for machining a hollow volume, 250 g of green powder was pressed. The quartz molds containing the pressed PVBVA-coated Aerosil were heated in air at 600 °C for 3 h to bake out the PVBVA, followed by heating in air at 1050 °C for 1.5 h to complete the sintering. The hollow volume sections of the cavity were prepared by machining the sintered Aerosil using a titanium-nitride-coated end mill. For light/tight mating of the cavity sections, each part was leveled on both sides by polishing on a glass plate with 240 grit SiC paper. An assembled cavity is shown in Figure 3.

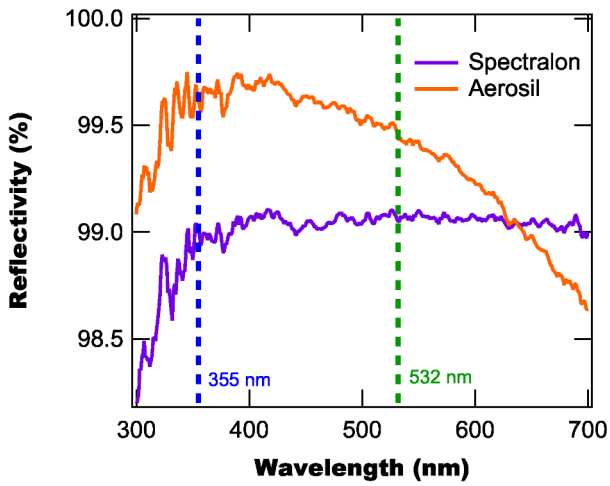

Figure 2. Absolute reflectivity curve of Aerosil cavity material with Spectralon reference curve for comparison.

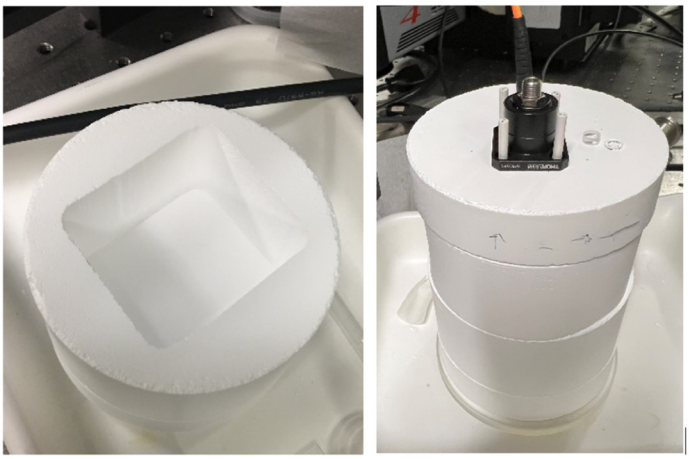

Figure 3. Images of the Aerosil cavity used for our ICERS experiments.

For spectroscopy in the integrating cavity, we used a frequency-tripled Nd:YAG laser (Photonics Industries DCH-355-5, 355 nm, 5 W average power, 0–200 kHz repetition rate, 9–51 ns pulse width, 0.7 mm) laser whose emission was coupled into a solarization-resistant silica fiber (Thorlabs FG400AEA, 0.22 NA, 400 µm, FC/PC connectors). The other end of the fiber was inserted into the cavity lid such that the tip of the fiber was even with the bottom of the lid. To collect the scattered light, we placed a lens tube into the cavity lid, which contained a 355 nm longpass filter (Semrock LP02-355RU-12.5-D, 279 cm^{-1} transition)

and coupling lens that coupled the collected light into a fiber bundle (round to linear, 19 × 200 μm high-OH fibers) attached to a spectrometer. The spectrometer consisted of a Princeton Instruments SP2500 monochromator (600 g/mm, 300 nm blaze, 100 μm slit) and a Princeton Instruments PI-Max 4 ICCD (1024i, 1024 × 1024, SB Phosphor). See Figure 1 for a schematic of the ICERs setup.

2.4. DUV Raman Spectroscopy

For DUV Raman spectroscopy (DUVRS), we utilize two different DUV sources: an OPOtek Radiant 355 HE OPO (<70 mJ, 10 Hz, 5 ns, 9 mm, 410 nm–2500 nm) and a frequency-tripled Coherent MIRA 900f Ti:sapphire oscillator (798 nm, 1.8 W, <115 fs, 76 MHz), which is pumped by a Coherent Verdi V10 Nd:YVO_4 laser (532 nm, 10 W, <5 MHz linewidth, RMS noise, 2%, 2 mm). The MIRA is tuned to 798 nm and then passed into a Harmonics box that contains nonlinear crystals that generate second harmonic (399 nm) and third harmonic (266 nm) light. Note that, since we are using an OPO and an fs-pulsed laser for our spectroscopy, the linewidths of the lasers are significantly larger than for a CW laser. For the OPO, we measure a linewidth of 6 cm^{-1}, and, for the MIRA, we measured the linewidths of the first, second, and third harmonics and find the linewidths to be 6 nm (95 cm^{-1}), 1.16 nm (69 cm^{-1}), and 0.52 nm (69 cm^{-1}), respectively.

For both lasers, the 266 nm emission is directed (using UV-protected aluminum mirrors) through a 50:50 UVFS plate beam splitter to a UVFS plano-convex focusing lens ($f = 40$ mm) that focuses the light onto the sample. The back-scattered light is then collected by the same lens and partially reflected by the beamsplitter through a 266 nm longpass filter (Semrock LP02-266RU-25, 372 cm^{-1} transition) and into a spectrometer. The spectrometer consists of a Princeton Instruments SP2300i monochromator (1800 g/mm holographic UV grating, slit 50 μm) and a Princeton Instruments PI-Max 3 ICCD (1024 × 256, UV). We center the monochromator at 281 nm to cover a relative wavenumber range of 87 cm^{-1} to 3652 cm^{-1} with a resolution of 12.6 cm^{-1}. See Figure 1 for a schematic of the DUVRS setup.

3. Results and Discussion

Before discussing the results of the novel Raman techniques, we first consider the results of a traditional Raman measurement using 532 nm excitation. Figure 4 displays the background- and fluorescence-subtracted Raman spectra from AY49-dyed nylon, AR337-dyed nylon, and pristine nylon. From Figure 4, we observe that nylon's strongest peak is near 2900 cm^{-1}, while AR337's strongest peak is at 1330 cm^{-1} and AY49's is at 1300 cm^{-1}. There are also many other peaks in the 800 cm^{-1} to 1800 cm^{-1} range, which correspond to various bonds (C-C, C-H, N-H, C=O, etc.).

3.1. THz Raman Spectroscopy

The first novel Raman technique we report on is THz Raman spectroscopy. After measuring the raw Raman spectrum, we performed background subtraction to remove residual signal near the Rayleigh line, with the resulting normalized spectra shown in Figure 5 for the pristine and dyed nylon. From Figure 5, we find that all three samples have similar spectra, with the only difference being a shift in the peak near 141 cm^{-1} and the relative intensity of some of the weaker peaks. These results suggest that neither of the dyes has vibrations in the THz regime, which was further confirmed by measuring the dyes in powder form. Note that the other dyes in Table 1 were also investigated for THz peaks, but none were found for any of these dyes. However, while the dyes have no THz peaks, they are found to affect nylon's 141 cm^{-1} peak, which is related to nylon's C-C torsion mode [37].

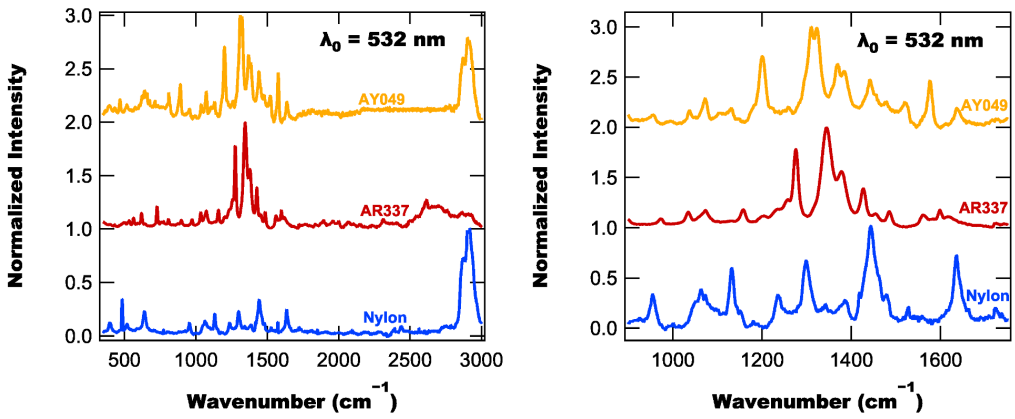

(**a**) (**b**)

Figure 4. Background and fluorescence subtracted Raman spectra of pristine nylon, AY49-dyed nylon, and AR337-dyed nylon measured using a standard Raman spectrometer and 532 nm excitation with (**a**) showing the full spectral range measured and (**b**) showing a zoomed in view of the 900 cm^{-1} to 1800 cm^{-1} range.

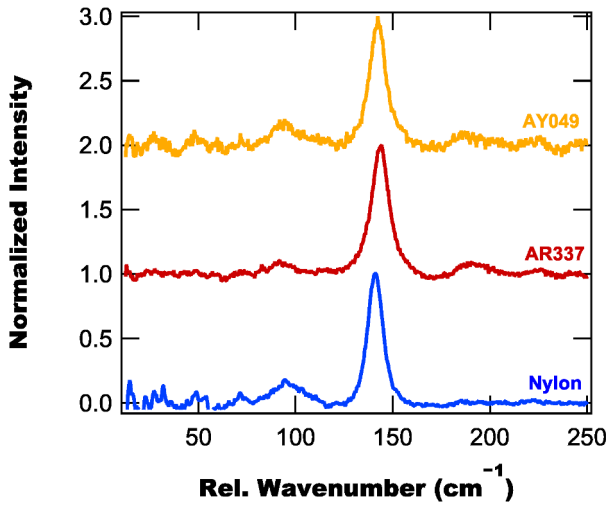

Figure 5. Background and fluorescence subtracted and normalized THz Raman spectra for both neat and dyed nylon.

3.2. ICERS

The next novel Raman technique we test is ICERS. We first characterized the cavity's average reflectivity at 355 nm and 532 nm using cavity ringdown measurements. The cavity's ringdown time τ is related to the average reflectivity $\overline{R}$ as [19]:

$$\overline{R} = e^{-\overline{d}/\tau}, \tag{1}$$

where $\overline{d}$ is the cavity's characteristic distance [19], which, for our cavity, is 2.185 cm. With Equation (1) and the measured ringdown times, we determined that the cavity had average reflectances of $R_{355} = 99.460 \pm 0.065\%$ and $R_{532} = 99.214 \pm 0.065\%$, which have theoretical cavity enhancements [25] of 185× and 127×, respectively.

Having confirmed sufficient cavity reflectivity to obtain noticable enhancement, we next performed ICERS measurements on pristine nylon, AY49-dyed nylon, and AR337-dyed nylon using both 532 nm and 355 nm excitation, with Figure 6a showing the spectra for 532 nm excitation and Figure 6b showing the spectra for 355 nm excitation. Note that the figure also includes the Raman spectrum of an empty cavity for reference.

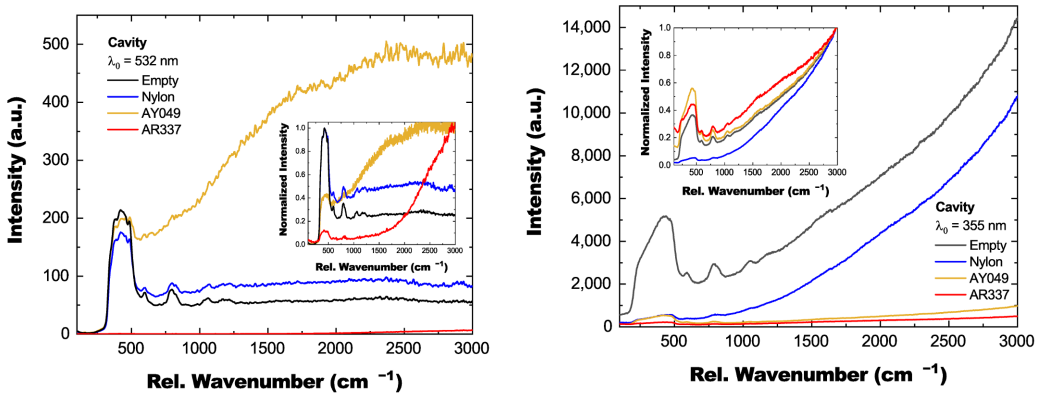

(**a**) (**b**)

Figure 6. Spectra measured from integrating cavity using 532 nm (**a**) and 355 nm (**b**) excitation for different nylon fibers and the empty cavity. Insets: normalized intensities.

From Figure 6a, we find that, for 532 nm excitation, the AR337-dyed sample displays little signal, while the AY49-dyed sample displays strong fluorescence emission (albeit with negligible Raman peaks). This difference in performance is due to the absorption spectra for the two fabrics. At 532 nm, the AR337-dyed nylon is strongly absorbing, such that the light scattering inside the cavity is quickly absorbed and does not allow for cavity enhancement. AY49, on the other hand, absorbs poorly at 532 nm, and, therefore, we do see some cavity enhancement of its signal. However, due to the fluorescence peak's location, the Raman peaks are overwhelmed by fluorescence.

Moving next to the 355 nm excitation, we find from Figure 6b that all three nylons display significantly less signal than the empty cavity's signal. This effect is due to all three nylons strongly absorbing at 355 nm, thus negating any possible cavity enhancement. Based on these observations (at 532 nm and 355 nm), it is obvious that the the ICERS technique is not suitable for samples that strongly absorb at the pump wavelength. However, given the observation of significant fluorescence signal for the AY49 sample using 532 nm, there is a possibility that using a wavelength that is not absorbed well could provide improvement. On the other hand, for dyed fibers, these wavelengths would typically be in the NIR, where the cavity reflectivities are significantly lower and the Raman intensities would be less (due to Raman scattering's dependence on λ^{-4} [17]). Therefore, it is unlikely that ICERS using UV/VIS excitation and the current cavity material will be a useful technique for fiber forensics. However, if a suitable cavity material is found with sufficient reflectivity in the NIR, it may be possible to take advantage of ICERS.

3.3. DUV Raman Spectroscopy

The final novel Raman technique we test is DUV Raman spectroscopy using 266 nm excitation. Based on this wavelength, we expect minimal fluorescence interference from the dyes and the Raman scattering to be 16× stronger than observed at 532 nm. Before measuring the dyed fibers, we first characterized the background spectra from the system (shown in Figure 7) using the MIRA and OPO. From Figure 7, we find strong Raman peaks from the fused silica optics (between 400 cm^{-1} and 1000 cm^{-1}) in addition to peaks from atmospheric oxygen (1555 cm^{-1}) and nitrogen (2350 cm^{-1}). Note that the atmospheric peaks are not observed for 532 nm excitation as 266 nm is resonant with O_2 and N_2, whereas 532 nm is not.

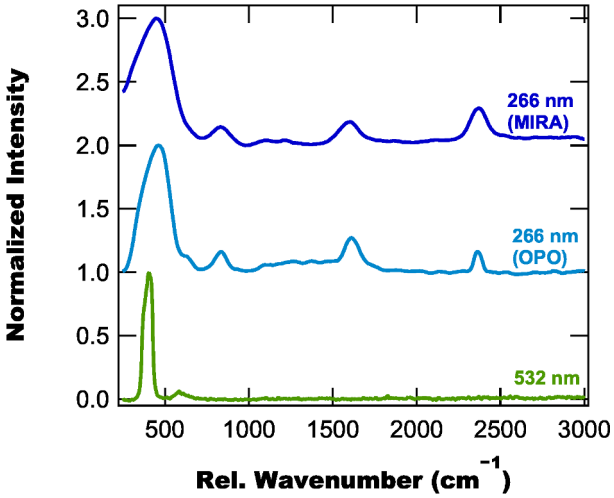

Figure 7. Comparison of background spectra measured using different lasers.

Having measured the DUV background spectra, we next measured the Raman spectra of the fabrics using OPO excitation, with Figure 8 showing the background and baseline subtracted spectra. From Figure 8, we find that the Raman spectra of all three nylons are essentially identical, with the peak positions found not to correspond to the expected dye's Raman peaks. This observation, along with the OPO's high intensity, suggests that the dyes and fabric undergo photodegradation when exposed to the high-intensity DUV excitation, with the resulting decay products of each material having similar Raman spectra.

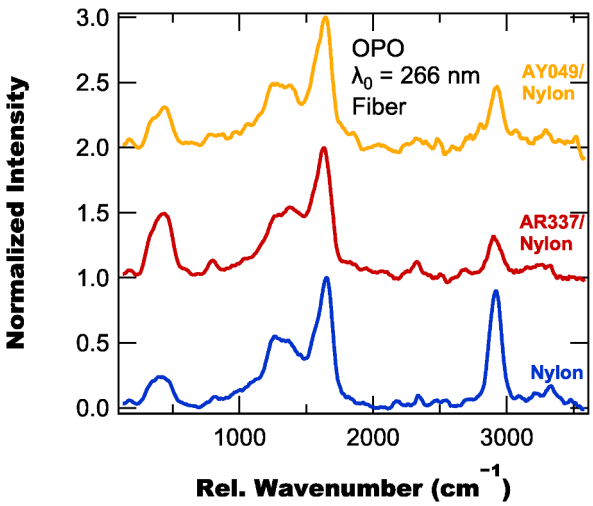

Figure 8. DUV Raman spectra of dyed nylons using OPO excitation.

Since the OPO was found to significantly degrade the sample, we next turned to the MIRA laser as it has a peak power of 0.526 kW and an average power of 5 mW, whereas the OPO had a peak power of 1000 kW and an average power of 100 mW. Despite the reduction in power, we once again found that the 266 nm excitation results in significant photodegradation over the timescale of the measurement, with the resulting decay products having similar Raman spectra (see Figure 9a). Note that we additionally performed tests where we further reduced the beam power using a waveplate–polarizer pair, but we were still unable to interrogate the sample without damage. It appears that the combination of the energetic DUV photons and strong absorbance of the samples make DUVRS infeasible for these materials.

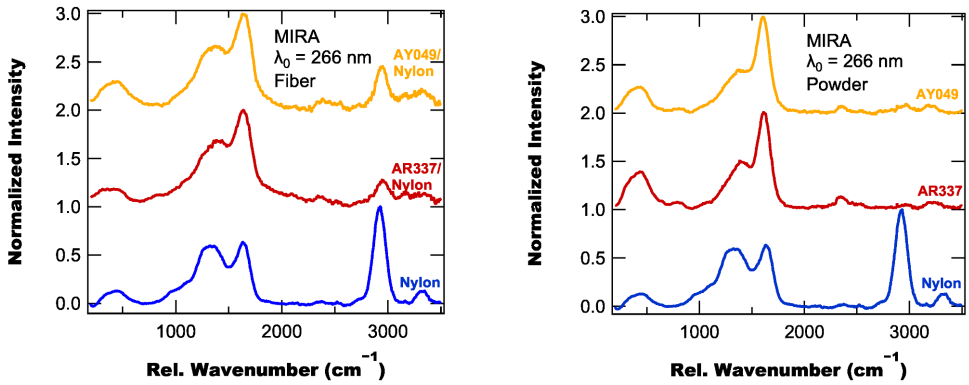

(**a**) (**b**)

Figure 9. Comparison of baseline subtracted DUV Raman spectra for fibers (**a**) and dye powder (**b**).

An Aside on Photodegradation

While the main goal of this paper is to evaluate novel Raman techniques for use in dyed-fabric forensics, it is worthwhile spending some time discussing the observed DUV photodegradation in further detail. Based on the similarity of the decayed nylons' Raman peaks, we first hypothesized that the spectra primarily arose from decay of the nylon (with the dye signature being too weak relative to the more plentiful host). However, when we tested this hypothesis by performing DUV Raman measurements on the dye powder, we found the surprising result that the dye powder displayed essentially the same Raman spectra (albeit missing nylon's peak at 2900 cm^{-1}), as shown in Figure 9b. This observation suggests that both dyes and the nylon undergo photodegradation into decay products that have similar Raman spectra. Note, however, that this similarity may only be a function of the deep-UV measurements using a broad radiation source and limited spectrometer resolution, such that unique peak structures are lost due to spectral broadening. In an effort to improve specificity, we also attempted Raman spectroscopy on the degraded materials using both 355 nm and 532 nm excitation. However, neither wavelength produced significant Raman scattering, which suggests that the degradation products are resonant at 266 nm but not at either 355 nm or 532 nm.

Despite our measurements' inability to provide better specificity, we can still make some initial chemical observations. Namely, based on the strong peak at ∼1670 cm^{-1}, we are most likely observing photobleaching via photooxidation as this peak is most likely due to the formation of C=O bonds [38,39].

4. Conclusions

We have tested three novel Raman techniques for dyed-fiber Raman spectroscopy—THz Raman spectroscopy (TRS), integrating-cavity-enhanced Raman spectroscopy (ICERS), and deep-UV Raman spectroscopy (DUVRS)—using a variety of dye-doped fabric samples, with particular focus on Acid Red 337 and Acid Yellow 49 dyed-nylon fibers. From our measurements, we find that the dyes do not display any significant peaks in the THz Raman region and, therefore, the technique is not overly useful for dyed-fabric identification. However, we do observe that the addition of the acid dyes to nylon can affect the peak position of the nylon's C-C torsion peak at 141 cm^{-1}.

For ICERS, we find that, while the technique can produce enhanced emission signals for low-absorbing media [23], the introduction of strong absorption breaks the technique as the scattered light in the cavity is quickly absorbed by the sample. Therefore, the usefulness of the cavity technique is limited to samples that do not absorb well at the excitation wavelength. As most dyes and fibers have absorbances in the UV and VIS, the natural solution would be to move towards NIR excitation. However, the cavity material's reflectivity is significantly lower in NIR and Raman scattering strength is

weaker at longer wavelengths, so the feasibility of NIR measurements—with this cavity material—is doubtful.

Finally, we tested DUVRS, which has the benefit of significantly stronger Raman scattering and Raman peaks that avoid the dyed fiber's fluorescence. While we did observe both benefits, we found that the Raman peaks we measured did not correspond to the dyed fiber's Raman peaks and instead are most likely due to photodegradation products of the dyed fiber. Regardless of how small of an intensity we interrogated the material with, we found that the dyed fibers would be significantly damaged by the DUV excitation during the measurement duration. The observation of rapid photodegradation of these materials using DUV excitation means that DUVRS is not a feasible technique for identifying most dyed fibers. However, there may be some dye–fiber combinations that are resistant to photodegradation in the DUV, but these will be a small subset of all the possible dye–fiber combinations.

Despite our initial goal of using novel Raman techniques to provide better tools for dyed-fiber forensic analysis, we find that all three techniques tested are actually worse than the current method of traditional Raman spectroscopy. Table 2 provides a comparison of these techniques, their theoretical promise, and the challenges identified in this study. These challenges are a function of the dye's lack of significant THz peaks, strong absorbance at the excitation wavelengths, and poor photodamage resistance in the DUV. While these techniques have proven inappropriate for dyed-fiber forensics, there are other novel Raman techniques that may prove useful in the field, including coherent anti-Stokes Raman spectroscopy (CARS) [40,41], stimulated Raman spectroscopy (SRS) [42], and surface-enhanced [43] or tip-enhanced [44] Raman spectroscopy (SERS or TERS). Additionally, assuming a suitable cavity material can be found with high reflectivity in the NIR, it may be possible to still use the ICERS technique with NIR excitation.

Table 2. Comparison of tested Raman techniques for application to dyed-fiber forensics.

	TRS	ICERS	DUVRS
Theoretical Promise	- Probing phonon modes for additional information to supplement traditional Raman measurements.	- Cavity enhancement of Raman intensity due to multiple scattering inside of the cavity.	- Increased intensity due to Raman scattering scaling as λ^{-4}. - Resonance enhancement due to UV absorption.
Challenges Identified	- Dyes tested in this study are found to have no THz peaks of their own.	- Dye absorbance at pump wavelength significantly reduces cavity enhancement. - For AY049, fluorescence was enhanced using 532 nm excitation, overwhelming any Raman signal.	- All samples tested displayed immediate photodegradation under exposure to DUV excitation, which destroyed the samples.
Future Outlook	- Identify any dyes that may have usable THz peaks. - Further investigation on the effects of dyes on the THz peaks of the host fabric.	- Cavity enhancement is possible for NIR excitation (e.g., 785 nm). However, a different cavity material is needed as the reflectivity of Aerosil falls off above 630 nm.	- This approach is unlikely to work as most organic dyes/fibers undergo photodegradation when exposed to DUV light.

Author Contributions: H.E. and B.R.A. conceived the experiments. N.G. prepared the integrating cavity. B.R.A. performed the experiments, data analysis, and wrote the manuscript with input from all authors. All authors have read and agreed to the published version of the manuscript.

Funding: This research was funded by the National Institute of Justice, Award #2018-DU-BX-0178.

Data Availability Statement: Data underlying the results presented in this paper are available from the authors upon reasonable request.

Acknowledgments: This work was supported by the National Institute of Justice, Award #2018-DU-BX-0178 to Washington State University. The authors would also like to thank Standard Colors and Nelson Vinueza (North Carolina State University) for providing the dyed fabrics used in this study.

Conflicts of Interest: The authors declare no conflict of interest.

References

1. Deedrick, D. *Hairs, Fibers, Crime, and Evidence Part 2: Fiber Evidence*; Forensics Science Communications 2, US Department of Justice, Federal Bureau of Investigation: Washington, DC, USA, 2000.
2. National Institute of Justice. *Trace Evidence*; National Institute of Justice: Washington, DC, USA, 2018.
3. Goodpaster, J.V.; Liszewski, E.A. Forensic analysis of dyed textile fibers. *Anal. Bioanal. Chem.* **2009**, *394*, 2009–2018. [CrossRef] [PubMed]
4. Buzzini, P. The characterization of textile fibers and other miscellaneous trace materials. In Proceedings of the Annual Meeting of the American Forensic Society, Seattle, WA, USA, 19–24 February 2018.
5. Buzzini, P.; Massonnet, G. The Analysis of Colored Acrylic, Cotton, and Wool Textile Fibers Using Micro-Raman Spectroscopy. Part 2: Comparison with the Traditional Methods of Fiber Examination. *J. Forensic Sci.* **2015**, *60*, 712–720. [CrossRef] [PubMed]
6. Massonnet, G. Raman spectroscopy and microspectrophotometry of reactive dyes on cotton fibres: Analysis and detection limits. *Forensic Sci. Int.* **2012**, *222*, 200–207. [CrossRef] [PubMed]
7. Robertson, C.R.J.; Wiggins, K.G. *Forensic Examination of Fibres*; CRC Press: Boca Raton, FL, USA, 2017.
8. Buzzini, P.; Suzuki, E. Forensic applications of Raman spectroscopy for the in situ analyses of pigments and dyes in ink and paint evidence. *J. Raman Spec.* **2016**, *47*, 16–27. [CrossRef]
9. Caycedo, M. Identification of Fifteen First Priority Textile Dyes from the Schweppe Collection with Raman and Surface Enhanced Raman Spectroscopy (SERS). Ph.D. Thesis, Universiteit van Amsterdam, Amsterdam, The Netherlands, 2012.
10. Cesaratto, A.; Centeno, S.A.; Lombardi, J.R.; Shibayama, N.; Leona, M. A complete Raman study of common acid red dyes: Application to the identification of artistic materials in polychrome prints. *J. Raman Spectrosc.* **2017**, *48*, 601–609. [CrossRef]
11. Was-Gubala, J.; Starczak, R. Nondestructive Identification of Dye Mixtures in Polyester and Cotton Fibers Using Raman Spectroscopy and Ultraviolet–Visible (UV-Vis) Microspectrophotometry. *Appl. Spectrosc.* **2015**, *69*, 296–303. [CrossRef]
12. Was-Gubala, J.; Machnowski, W. Application of Raman Spectroscopy for Differentiation Among Cotton and Viscose Fibers Dyed with Several Dye Classes. *Spectrosc. Lett.* **2014**, *47*, 527–535. [CrossRef]
13. Puchowicz, D.; Cieslak, M. Raman Spectroscopy in the Analysis of Textile Structures. In *Recent Developments in Atomic Force Microscopy and Raman Spectroscopy for Materials Characterization*; IntechOpen: London, UK, 2022.
14. Massonnet, G.; Buzzini, P.; Jochem, G.; Stauber, M.; Coyle, T.; Roux, C.; Thomas, J.; Leijenhorst, H.; Zanten, Z.V.; Wiggins, K.; et al. Evaluation of Raman Spectroscopy for the Analysis of Colored Fibers: A Collaborative Study. *J. Forensic Sci.* **2005**, *50*, 1028–1038. [CrossRef]
15. Thomas, J.; Buzzini, P.; Massonnet, G.; Reedy, B.; Roux, C. Raman spectroscopy and the forensic analysis of black/grey and blue cotton fibres. *Forensic Sci. Int.* **2005**, *152*, 189–197. [CrossRef]
16. Buzzini, P.; Massonnet, G. The Discrimination of Colored Acrylic, Cotton, and Wool Textile Fibers Using Micro-Raman Spectroscopy. Part 1: In situ Detection and Characterization of Dyes. *J. Forensic Sci.* **2013**, *58*, 1593–1600. [CrossRef]
17. Menzel, R. *Photonics*, 2nd ed.; Springer: Berlin/Heidelberg, Germany, 2007.
18. Menezes, D.B.; Reyer, A.; Yaksel, A.; Oliveira, B.B.; Musso, M. Introduction to Terahertz Raman spectroscopy. *Spectrosc. Lett.* **2018**, *51*, 438–445. [CrossRef]
19. Cone, M.T.; Musser, J.A.; Figueroa, E.; Mason, J.D.; Fry, E.S. Diffuse reflecting material for integrating cavity spectroscopy, including ring-down spectroscopy. *Appl. Opt.* **2015**, *54*, 334. [CrossRef]
20. Bixler, J.N.; Winkler, C.A.; Hokr, B.H.; Mason, J.D.; Yakovlev, V.V. Utilizing scattering to further enhance integrating cavity-enhanced spectroscopy. *J. Mod. Opt.* **2016**, *63*, 76–79. [CrossRef]
21. Cone, M.T.; Mason, J.D.; Figueroa, E.; Hokr, B.H.; Bixler, J.N.; Castellanos, C.C.; Noojin, G.D.; Wigle, J.C.; Rockwell, B.A.; Yakovlev, V.V.; et al. Measuring the absorption coefficient of biological materials using integrating cavity ring-down spectroscopy. *Optica* **2015**, *2*, 162. [CrossRef]
22. Moore, T.Z.; Yakovlev, V.V.; Mason, J.D.; Tedford, V.; Fry, E.S.; Favela, K.A.; Nodurft, D.T. Chemical, biological, and trace gas detection and measurement with a newly developed integrating Cavity Enhanced Raman (iCERS) technique. In *Next-Generation Spectroscopic Technologies XI*; SPIE: Bellingham, WA, USA, 2018.
23. Moore, T.Z.; Yakovlev, V.V.; Mason, J.D.; Fry, E.S.; Nodurft, D.T.; Tedford, V.; Favela, K.A. Integrating Cavity Enhanced Raman Spectroscopyof Trace Gases and Bulk Compounds. In *CLEO*; Optica Publishing Group: Washington, DC, USA, 2019; p. JTh2A.87.
24. Niklas, C.; Wackerbarth, H.; Ctistis, G. A Short Review of Cavity-Enhanced Raman Spectroscopy for Gas Analysis. *Sensors* **2021**, *21*, 1698. [CrossRef]
25. Saleh, B.; Teich, M. *Fundamentals of Photonics*, 1st ed.; Wiley: Hoboken, NJ, USA, 1991.

26. Relman, D. Detection and Identification of Previously Unrecognized Microbial Pathogens. *Emerg. Infect. Dis.* **1998**, *4*, 382–389. [CrossRef]
27. Nelson, W.H.; Manoharan, R.; Sperry, J.F. UV Resonance Raman Studies of Bacteria. *Appl. Spectrosc. Rev.* **1992**, *27*, 67–124. [CrossRef]
28. Christesen, S.D.; Lochner, J.M.; Hyre, A.M.; Emge, D.K.; Jones, J.P. UV Raman spectra and cross sections of chemical agents. In *Chemical and Biological Sensing VII*; SPIE: Bellingham, WA, USA, 2006.
29. Hug, W.F.; Bhartia, R.; Taspin, A.; Lane, A.; Conrad, P.; Sijapati, K.; Reid, R.D. Status of miniature integrated UV resonance fluorescence and Raman sensors for detection and identification of biochemical warfare agents. In *Chemical and Biological Sensors for Industrial and Environmental Security*; SPIE: Bellingham, WA, USA, 2005.
30. Asher, S.A.; Johnson, C.R. Raman Spectroscopy of a Coal Liquid Shows That Fluorescence Interference Is Minimized with Ultraviolet Excitation. *Science* **1984**, *225*, 311–313. [CrossRef]
31. Jakubek, R.S.; Handen, J.; White, S.E.; Asher, S.A.; Lednev, I.K. Ultraviolet resonance Raman spectroscopic markers for protein structure and dynamics. *TrAC Trends Anal. Chem.* **2018**, *103*, 223–229. [CrossRef]
32. Chinsky, L.; Jolles, B.; Laigle, A.; Turpin, P.Y. Resonance Raman spectra of poly(L-lysine), aromatic amino acids, L-histidine and native and thermally unfolded ribonuclease A. *J. Raman Spectrosc.* **1985**, *16*, 235–241. [CrossRef]
33. Nagli, L.; Gaft, M.; Fleger, Y.; Rosenbluh, M. Absolute Raman cross-sections of some explosives: Trend to UV. *Opt. Mater.* **2008**, *30*, 1747–1754. [CrossRef]
34. El-Abassy, R.M.; von der Kammer, B.; Materny, A. UV Raman spectroscopy for the characterization of strongly fluorescing beverages. *LWT-Food Sci. Technol.* **2015**, *64*, 56–60. [CrossRef]
35. Wu, M.; Ray, M.; Fung, K.H.; Ruckman, M.W.; Harder, D.; Sedlacek, A.J. Stand-off Detection of Chemicals by UV Raman Spectroscopy. *Appl. Spectrosc.* **2000**, *54*, 800–806. [CrossRef]
36. Li, B.; Myers, A.B. Absolute Raman cross sections for cyclohexane, acetonitrile, and water in the far-ultraviolet region. *J. Phys. Chem.* **1990**, *94*, 4051–4054. [CrossRef]
37. Shukla, S.K.; Kumar, N.; Mishra, A.K.; Tandon, P.; Gupta, V.D. Normal Modes and Their Dispersion in α Form of Nylon-6 (αNY6). *Polym. J.* **2007**, *39*, 359–368. [CrossRef]
38. Aldrich, S. IR Spectrum Table & Chart. Available online: https://www.sigmaaldrich.com/US/en/technical-documents/technical-article/analytical-chemistry/photometry-and-reflectometry/ir-spectrum-table (accessed on 18 October 2021).
39. Matsui, H.; Arrivo, S.M.; Valentini, J.J.; Weber, J.N. Resonance Raman Studies of Photoinduced Decomposition of Nylon-6,6: Product Identification and Mechanistic Determination. *Macromolecules* **2000**, *33*, 5655–5664. [CrossRef]
40. Maker, P.D.; Terhune, R.W. Study of Optical Effects Due to an Induced Polarization Third-Order in the Electric Field Strength. *Phys. Rev.* **1965**, *137*, 801–818. [CrossRef]
41. Tolles, W.M.; Nibler, J.W.; McDonald, J.R.; Harvey, A.B. A Review of the Theory and Application of Coherent Anti-Stokes Raman Spectroscopy (CARS). *Appl. Spectrosc.* **1977**, *31*, 253–271. [CrossRef]
42. Prince, R.C.; Frontiera, R.R.; Potma, E.O. Stimulated Raman Scattering: From Bulk to Nano. *Chem. Rev.* **2017**, *117*, 5070–5094. [CrossRef]
43. Lombardi, J.R.; Birke, R.L. A Unified Approach to Surface-Enhanced Raman Spectroscopy. *J. Phys. Chem. C* **2008**, *112*, 5605–5617. [CrossRef]
44. Anderson, M.S. Locally enhanced Raman spectroscopy with an atomic force microscope. *Appl. Phys. Lett.* **2000**, *76*, 3130–3132. [CrossRef]